JASA ARTICLE

Active structural acoustic control using an experimentally identified radiation resistance matrix

Joseph Milton, Jordan Cheer,[a] and Steve Daley
Institute of Sound and Vibration Research, University of Southampton, Southampton, SO17 1BJ, United Kingdom

ABSTRACT:
Active structural acoustic control (ASAC) is a widely used active noise control technique that provides control of structurally radiated noise through actuation of the radiating structure. Typically, ASAC drives structural actuators to minimise a real-time measurement of the radiated sound field. However, it is often not practical to position error microphones in the radiated sound field. To overcome this limitation, a number of methods have previously been proposed. One such method utilises the radiation resistance matrix to map structural response measurements to the acoustic response and, thus, enable an estimate of the structurally radiated sound power from structural measurements alone. This has previously relied upon precise modelling of the radiating structure which, for practical structures, can lead to limitations in the accuracy of the estimate. In this paper, an ASAC strategy that utilises an experimentally identified radiation resistance matrix is presented. The robustness of both the sound power estimation and the ASAC controller to system uncertainties is investigated, and it has been shown that the proposed ASAC strategy is able to achieve effective control of the radiated sound power.
https://doi.org/10.1121/10.0000858
(Received 16 December 2019; revised 5 February 2020; accepted 19 February 2020; published online 5 March 2020)
[Editor: Nicole Kessissoglou] Pages: 1459–1468

I. INTRODUCTION

Active structural acoustic control (ASAC) is an effective and lightweight solution for structure-borne sound radiation and transmission problems. Generally speaking, ASAC aims to minimise the sound pressure measured at an array of error sensors located in the radiated sound field by controlling structural vibrations using a distribution of structural actuators. The application of such a system, however, can be limited for a number of reasons, which include the robustness of sensitive acoustic error sensors, the practicality of placing acoustic error sensors, and the discrete location of the error sensors, and therefore, at higher frequencies, the limited global acoustic control. A number of ASAC systems have recently been developed that aim to overcome some or all of these limitations by focusing on reducing the radiated sound power, which, when minimised, ensures a global reduction. However, measuring the radiated sound power directly is not straightforward, and thus a number of publications have proposed different approaches to controlling the structurally radiated sound power using only structural measurements.[1–7]

One such approach recently proposed uses the weighted sum of spatial gradients (WSSG) to attempt to control the structural radiation.[7,8] The WSSG can be measured using a closely spaced array of four accelerometers, and it has been shown that this provides a uniform measure across the surface of a plate. Therefore, the WSSG sensor is insensitive to its location and does not require *a priori* knowledge of the structure.[7] The WSSG control method has been shown through both simulations and experiments to provide effective control of the sound power radiated from a flat plate.[7] More recently, the method has been extended to a cylindrical structure,[8] where it has been shown to provide close to optimal sound power control in numerical simulations. However, its performance during experiments conducted using a practical cylindrical structure has been shown to have some limitations due to discrepancies between the structural properties and assumed boundary conditions.[8] Nevertheless, the WSSG method does potentially provide an ASAC method that is convenient to implement in practice, requiring only a small number of error sensors, even if multiple WSSG sensors are required to improve the practical robustness.

Several alternative approaches to implementing ASAC using only structural sensors include the use of the radiation resistance matrix,[2,4] which is able to completely describe the radiation from a structure in terms of its radiation modes.[1] In this previous work, the radiation resistance matrix has been calculated using a variety of different methods. For example, a number of publications have focused on using analytical or numerical modelling to estimate the radiation resistance matrix.[4,9,10] These model-based methods often rely on specific assumptions about the radiating structure, and this limits their practical performance.

These practical limitations have been addressed by various publications that propose different methods to identify the radiation resistance matrix experimentally.[6,11] Koopmann and Fahnline, for example, developed a method to measure the elements of the radiation resistance matrix using a bespoke

[a]Electronic mail: J.Cheer@soton.ac.uk, ORCID: 0000-0002-0552-5506.

measurement probe, consisting of a loudspeaker and microphone, called the resistance probe.[11] This method relies on the probe generating a known volume velocity on the surface of the structure and a collocated measurement of the pressure. To achieve an accurate measurement at higher frequencies, the probe must be sufficiently small so that it represents a small area of the radiating structure. However, this conflicts with the requirement to generate sufficiently high volume velocity at low frequencies. These opposing requirements mean that the method has been shown to have a low frequency limit of around 200 Hz and, therefore, may have limited applicability in situations where active control would be appropriate.

Alternative methods of experimentally identifying the radiation resistance matrix have focused on the formulation and solution of a variety of inverse problems. For example, Berkhoff proposed a method that uses the responses measured between a number of structural forces and distributions of both structural velocity and acoustic pressure measurements to estimate the radiation resistance matrix.[6] This method has been shown to be effective experimentally. However, since measurements of the acoustic pressure are used to calculate the radiated sound power, the radiating structure must be located in a free-field acoustic environment and the pressure measurements must be taken in the far-field. This may be infeasible for many practical structures, which cannot be relocated to a free-field acoustic environment. To overcome this problem, an alternative inverse problem–based method has been proposed that identifies the radiation resistance matrix experimentally using the responses measured between a distribution of structural forces and an array of structural velocity and near-field acoustic pressure and particle velocity measurements.[12] This method has been shown to accurately estimate both the sound power level and resonance frequencies of the radiating modes when using at least eight forces and both structural and acoustic sensors per acoustic wavelength.

This paper investigates how the radiation resistance matrix identified according to the experimental method proposed in Ref. 12 can be utilised in an ASAC system to estimate and control the radiated sound power. For completeness, Sec. II summarises the formulation and method to experimentally identify the radiation resistance matrix according to the method proposed in Ref. 12. Section III formulates the standard active vibration control (AVC) and proposed ASAC strategies, which include a modification of the radiation resistance matrix to ensure convergence. In Sec. IV, a practical radiation control problem is defined and, in the first instance, an estimate of the radiated sound power is calculated using the experimentally identified radiation resistance matrix. The robustness of this estimate is then assessed when random uncertainties are introduced into both the structural and acoustic responses of the system. The performance of the proposed ASAC strategy is then compared to that of an equivalent AVC strategy, using the optimal control performance calculated offline utilising measured responses. The robustness of each control strategy is also investigated for the case when random uncertainties are introduced into the physical responses. In Sec. V, the proposed ASAC strategy is validated experimentally in real-time, and then Sec. VI draws conclusions based on the presented results.

II. EXPERIMENTAL IDENTIFICATION OF THE RADIATION RESISTANCE MATRIX

In this section, the formulation for the experimental identification of the radiation resistance matrix is described, as previously presented by Milton *et al.*[12]

The sound power radiated from a structure at a single frequency can be expressed in terms of the vectors of particle velocities, $\mathbf{v}$, and acoustic pressures, $\mathbf{p}$, measured over a virtual surface enclosing the structure as

$$W = \left(\frac{A}{2}\right)\mathrm{Re}\{\mathbf{p}^H\mathbf{v}\}, \tag{1}$$

where A is the area over which the particle velocities and acoustic pressures are measured, divided by the number of measurement positions.[13] These acoustic pressures and particle velocities can be expressed in terms of the structural responses as

$$\mathbf{p} = \tilde{\mathbf{H}}_p\mathbf{q}, \quad \text{and} \quad \mathbf{v} = \tilde{\mathbf{H}}_v\mathbf{q}, \tag{2}$$

where $\mathbf{q}$ is the vector of structural responses measured on the surface of the structure, and $\tilde{\mathbf{H}}_p$ and $\tilde{\mathbf{H}}_v$ are the transfer response matrices between the structural responses and the acoustic pressures and particle velocities, respectively. It should be noted that the structural responses, $\mathbf{q}$, can be represented by accelerations, velocities, or displacements. Substituting Eq. (2) into Eq. (1) for the acoustic pressures and particle velocities, the radiated sound power can be written in terms of the measured structural responses as

$$W = \left(\frac{A}{2}\right)\mathrm{Re}\left\{\mathbf{q}^H\tilde{\mathbf{H}}_p^H\tilde{\mathbf{H}}_v\mathbf{q}\right\}. \tag{3}$$

Expanding this in terms of its real and imaginary parts allows a simplification that gives

$$W = \left(\frac{A}{4}\right)\mathbf{q}^H[\Xi^H + \Xi]\mathbf{q} = \mathbf{q}^H\mathbf{R}\mathbf{q}, \tag{4}$$

where $\Xi = \tilde{\mathbf{H}}_p^H\tilde{\mathbf{H}}_v$ and the experimentally identified radiation resistance matrix is defined as

$$\mathbf{R} = (A/2)\mathrm{Re}\left[\tilde{\mathbf{H}}_p^H\tilde{\mathbf{H}}_v\right]. \tag{5}$$

Although Eq. (5) defines the radiation resistance matrix, the matrices $\tilde{\mathbf{H}}_p$ and $\tilde{\mathbf{H}}_v$ cannot be measured directly since each of the structural responses cannot be independently driven and are only controllable via a fully coupled transfer response matrix.[5] However, it is possible to estimate these matrices via the solution of an inverse problem.[5,12,14–16] This inverse problem can be formulated by expressing the structural responses, $\mathbf{q}$, in terms of a distribution of structural forces, $\mathbf{f}$, and a transfer response matrix as

https://doi.org/10.1121/10.0000858

$$\mathbf{q} = \mathbf{H}_s\mathbf{f}, \tag{6}$$

where $\mathbf{H}_s$ is the transfer response matrix measured between the distribution of independently driven forces and the structural responses, which *can* be measured directly. The relationships between the three transfer responses and the vectors of forces, structural responses, acoustic pressures, and particle velocities are summarised by the block diagram shown in Fig. 1. From this block diagram, or by substituting Eq. (6) into Eq. (2), it can be seen that the acoustic pressure and particle velocity vectors can be expressed as

$$\mathbf{p} = \tilde{\mathbf{H}}_p\mathbf{H}_s\mathbf{f} = \mathbf{H}_p\mathbf{f} \quad \text{and} \quad \mathbf{u} = \tilde{\mathbf{H}}_v\mathbf{H}_s\mathbf{f} = \mathbf{H}_v\mathbf{f}, \tag{7}$$

where $\mathbf{H}_p$ and $\mathbf{H}_v$ are the matrices of transfer responses between the forces and the acoustic pressures and particle velocities, respectively. The matrices $\tilde{\mathbf{H}}_p$ and $\tilde{\mathbf{H}}_v$ can then be obtained via the solutions to the two corresponding inverse problems, that is,

$$\tilde{\mathbf{H}}_p = \mathbf{H}_p\mathbf{H}_s^{\dagger} \quad \text{and} \quad \tilde{\mathbf{H}}_v = \mathbf{H}_v\mathbf{H}_s^{\dagger}, \tag{8}$$

where the superscript "†" denotes the pseudo-inverse operator. The particular solution to the pseudo-inverse is dependent on the dimensions of the structural response matrix, $\mathbf{H}_s$, and the possible solutions are explained in detail in Ref. 12.

III. ACTIVE STRUCTURAL CONTROL STRATEGIES

In this section, two active structural control strategies are formulated. The first, AVC, aims to minimise the sum of the squared error signals measured on the surface of a structure directly, and the second, the proposed ASAC strategy, aims to minimise an estimate of the radiated sound power calculated using error measurements taken on the surface of the structure along with the experimentally identified radiation resistance matrix. The AVC strategy is used as a benchmark when assessing the performance and robustness of the proposed control strategy.

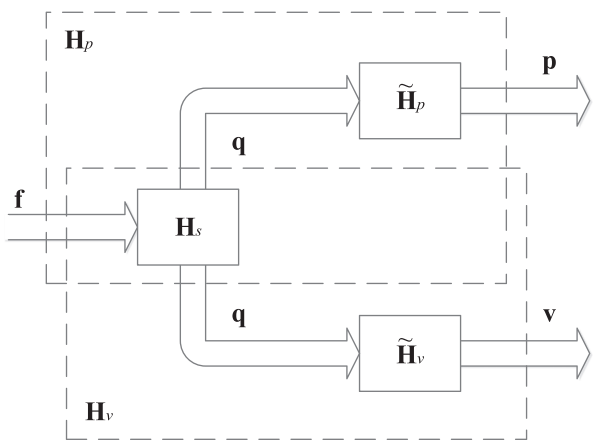

FIG. 1. Block diagram showing how the transfer responses, $\mathbf{H}_s$, $\mathbf{H}_p$, $\mathbf{H}_v$, $\tilde{\mathbf{H}}_p$, and $\tilde{\mathbf{H}}_v$ relate to the forces, $\mathbf{f}$, structural responses, $\mathbf{q}$, particle velocities, $\mathbf{v}$, and acoustic pressures, $\mathbf{p}$ (Ref. 12).

A. AVC

The considered AVC system aims to minimise the sum of the squared signals measured at L_s structural error sensors. This can be defined at a single frequency by the cost function

$$J_s = \mathbf{e}^H\mathbf{e}, \tag{9}$$

where $\mathbf{e}$ is the vector of L_s error signals in the steady state, measured on the surface of the plate. The vector of error signals, $\mathbf{e}$, can be expressed as the linear superposition of the primary disturbance measured at each sensor position and the contribution due to the controller, which gives

$$\mathbf{e} = \mathbf{d} + \mathbf{G}\mathbf{u}, \tag{10}$$

where $\mathbf{d}$ is the vector of L_s primary disturbances, $\mathbf{u}$ is the vector of M control signals, and $\mathbf{G}$ is the $(L_s \times M)$ matrix of transfer responses measured between the control actuators and the error sensors. By substituting Eq. (10) into Eq. (9), the cost function can be written as

$$J_s = \mathbf{u}^H\mathbf{G}^H\mathbf{G}\mathbf{u} + \mathbf{d}^H\mathbf{G}\mathbf{u} + \mathbf{u}^H\mathbf{G}^H\mathbf{d} + \mathbf{d}^H\mathbf{d}. \tag{11}$$

If the matrix $\mathbf{G}^H\mathbf{G}$ is assumed to be positive definite, which is generally the case,[17] then the control signals that minimise the cost function, J_s, are generated by setting the derivative of Eq. (11) with respect to the real and imaginary parts of $\mathbf{u}$ to zero. The optimal vector of control signals is then

$$\mathbf{u}_{\text{opt}}^{(\text{AVC})} = -\left[\mathbf{G}^H\mathbf{G} + \beta\mathbf{I}\right]^{-1}\mathbf{G}^H\mathbf{d}, \tag{12}$$

where β is a regularization term that introduces a limit on the control effort, and $\mathbf{I}$ is the identity matrix.

For practical applications, the disturbance signals are not known in advance and therefore, to minimise the sum of the squared error signals in real-time, an algorithm that is able to iteratively adjust the input to the control actuators, $\mathbf{u}$, is needed. In this case, the method of steepest descent has been used to manipulate the measured signals and drive the control actuators to minimise the sum of the squared error signals. This update algorithm is written as

$$\mathbf{u}(n+1) = \gamma\,\mathbf{u}(n) - \alpha\,\widehat{\mathbf{G}}^H\,\mathbf{e}(n), \tag{13}$$

where n represents the current iteration step of the algorithm, $\widehat{\mathbf{G}}$ is an estimate of the plant response matrix, γ is the leakage factor, and α is the convergence gain. The leakage factor, regularization coefficient, and convergence coefficient can be related as[17]

$$\beta = \frac{(1-\gamma)}{\alpha}. \tag{14}$$

A block diagram showing the adaptive implementation of the AVC algorithm is shown in Fig. 2.

B. ASAC

The proposed ASAC strategy utilises the experimentally identified radiation resistance matrix, along with

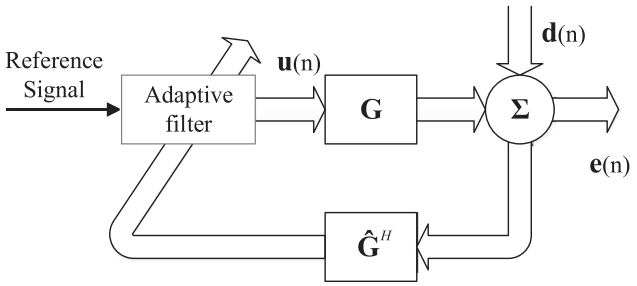

FIG. 2. Block diagram of the feedforward AVC system described by Eq. (12).

structural error measurements, to minimise a cost function that estimates the structurally radiated sound power. Using the radiation resistance matrix, along with the vector of error signals measured on the surface of the plate, the cost function in this case is given, following Eq. (4), as

$$J_W = \mathbf{e}^H \mathbf{R} \mathbf{e}. \tag{15}$$

Whilst the radiation resistance matrix, $\mathbf{R}$, can be used to estimate the radiated sound power from an excited structure,[12,13] as in Eq. (4), it is not guaranteed to be positive definite. This means that the cost function defined in Eq. (15) is not guaranteed to have a global minimum. For this reason, further steps must be taken in order to enforce positive definiteness on the radiation resistance matrix.

This problem has been approached previously for a broadband control system[5] by calculating a linear time invariant (LTI) model of a power transfer matrix via a non-convex optimisation procedure, followed by further optimisation to ensure positive definiteness. However, for tonal control, this method is overly complex and likely to limit the performance and stability of the control system when excited off-resonance due to limitations in the accuracy of the LTI model. For the tonal radiation problem considered here, these limitations can be overcome via direct calculation of the nearest positive semi-definite matrix approximation of the radiation resistance matrix from the frequency response data. This approximant can then be used in place of $\mathbf{R}$ in Eq. (15) so that the cost function has a single global minimum.

The nearest positive semi-definite matrix that approximates the radiation resistance matrix can be found using one of two methods, which use either the two-norm or Frobenius norm method.[18] In this study, the latter method has been used as it is less computationally demanding.[15] The nearest positive semi-definite matrix is given according to the Frobenius norm by minimising

$$||\mathbf{R} - \widehat{\mathbf{R}}||_F^2, \tag{16}$$

where $||\ldots||_F$ is the Frobenius norm,[19] and $\widehat{\mathbf{R}}$ is the positive semi-definite approximant of the radiation resistance matrix, $\mathbf{R}$. The solution in this case is[18]

$$\widehat{\mathbf{R}} = \frac{\mathbf{B} + \mathbf{H}}{2}, \tag{17}$$

where the symmetric part of $\mathbf{R}$ is given by $\mathbf{B} = (\mathbf{R} + \mathbf{R}^H)/2$, and the positive Hermitian matrix, $\mathbf{H}$, is given by the polar decomposition of $\mathbf{B}$, which is given as $\mathbf{B} = \mathbf{U}\mathbf{H}$, where $\mathbf{U}^T\mathbf{U} = 1$ and $\mathbf{H}^T\mathbf{H} \geq 0$. Alternatively, the symmetric positive semi-definite radiation resistance matrix, $\widehat{\mathbf{R}}$, can be calculated from the eigenvalue decomposition of $\mathbf{B}$, which is given as[18]

$$\mathbf{B} = \mathbf{Z}\Lambda\mathbf{Z}^{-1}, \tag{18}$$

where $\mathbf{Z}$ is the matrix of eigenvectors and Λ is the diagonal matrix of eigenvalues, λ_i The positive semi-definite approximant of the radiation resistance matrix, $\mathbf{R}$, is then

$$\widehat{\mathbf{R}} = \mathbf{Z}\mathbf{Y}\mathbf{Z}^{-1}, \tag{19}$$

where $\mathbf{Y}$ is the diagonal matrix formed from the eigenvalues of Λ according to the rule

$$y_i = \lambda_i, \text{ if } \lambda_i \geq 0, \quad \text{and} \quad y_i = 0, \text{ if } \lambda_i < 0. \tag{20}$$

That is, $\mathbf{Y}$ contains the positive eigenvalues of $\widehat{\mathbf{R}}$ and the negative eigenvalues are set to zero.

Using the positive semi-definite approximant of the radiation resistance matrix, the cost function defined in Eq. (15) can be rewritten to ensure that it has a single global minimum as

$$J_W = \mathbf{e}^H \widehat{\mathbf{R}} \mathbf{e}, \tag{21}$$

where $\widehat{\mathbf{R}}$ is the positive semi-definite approximant of the radiation resistance matrix. By substituting Eq. (10) for the structural error signals into Eq. (21) and expanding, the cost function becomes

$$J_W = (\mathbf{d} + \mathbf{G}\mathbf{u})^H \widehat{\mathbf{R}} (\mathbf{d} + \mathbf{G}\mathbf{u}) \tag{22}$$

$$= \mathbf{u}^H \mathbf{G}^H \widehat{\mathbf{R}} \mathbf{G}\mathbf{u} + \mathbf{d}^H \widehat{\mathbf{R}} \mathbf{G}\mathbf{u} + \mathbf{u}^H \mathbf{G}^H \widehat{\mathbf{R}} \mathbf{d} + \mathbf{d}^H \widehat{\mathbf{R}} \mathbf{d}. \tag{23}$$

As for AVC, the vector of optimal control signals, $\mathbf{u}_{\text{opt}}^{(\text{ASAC})}$, is obtained by setting the derivative of Eq. (23) with respect to the real and imaginary parts of $\mathbf{u}$ to zero, which gives the vector of optimal control signals in this case as

$$\mathbf{u}_{\text{opt}}^{(\text{ASAC})} = -\left[\mathbf{G}^H \widehat{\mathbf{R}} \mathbf{G} + \beta \mathbf{I}\right]^{-1} \mathbf{G}^H \widehat{\mathbf{R}} \mathbf{d}, \tag{24}$$

where the regularization term has again been introduced to limit the control effort.

As in Sec. III A, in practice, since the disturbance signals are not generally known in advance, an iterative algorithm is required to minimise the cost function. The steepest descent update algorithm in this case is given as

$$\mathbf{u}(n+1) = \gamma \mathbf{u}(n) - \alpha \widehat{\mathbf{G}}^H \widehat{\mathbf{R}}\, \mathbf{e}(n), \tag{25}$$

where it can be seen that the approximant of the radiation resistance matrix operates as a complex weighting on the vector of error signals. A block diagram showing the adaptive implementation of this ASAC algorithm is shown in Fig. 3.

https://doi.org/10.1121/10.0000858

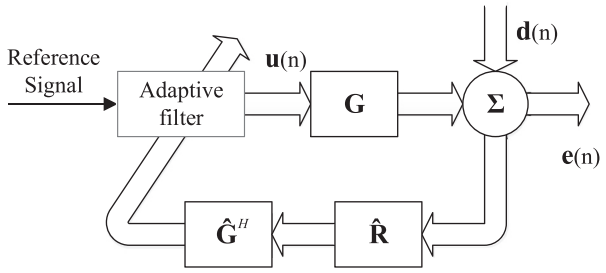

FIG. 3. Block diagram of the feedforward ASAC system described by Eq. (25).

IV. CONTROL OF RADIATION FROM A FLAT PLATE

In this section, the experimental setup used to investigate the performance of the proposed ASAC strategy is first described. The radiation resistance matrix for this structure is then identified, and an estimate of the sound power is calculated. The robustness of this sound power estimate to uncertainty in both the structural and acoustic responses is then investigated. The performance of both AVC and the proposed ASAC system are nextcalculated for the optimal cases offline using the measured system responses, and the robustness of the two control strategies is then investigated through the addition of uncertainty into the physical responses.

A. System description

The radiating structure considered in this paper is a flat aluminium plate of dimensions 0.414 m by 0.314 m, coupled to a rigid enclosure, as shown in Fig. 4. A distribution of 12 lightweight inertial actuators, arranged as shown in Fig. 4, has been fixed to the surface of the plate. These actuators provide both the forces required to identify the radiation resistance matrix, as detailed in Sec. II, and the control forces used by the control strategies formulated in Sec. III. Each actuator was approximately collocated with an accelerometer, which was used to provide the required measure of the structural response. The pressure and particle velocity were measured above each accelerometer position, approximately 10 cm from the surface of the plate, using a Microflown PU probe (The Netherlands) The primary disturbance was provided by a loudspeaker located inside of the enclosure, as shown in Fig. 4.

In order to validate the accuracy of the sound power measurements using the planar grid of 12 sensor positions, a preliminary study was carried out in which the radiated sound power was measured according to BS EN ISO 9614 over a hemispherical surface with 72 sensor positions fully enclosing the experimental rig.[20] This preliminary study confirmed that the adopted sound power measurement method was accurate over the frequency range 60–350 Hz. Therefore, to avoid the time-consuming nature of setting up the fine grid of sensor positions on a hemispherical surface for each of the control scenarios, the planar sensor array was utilised.

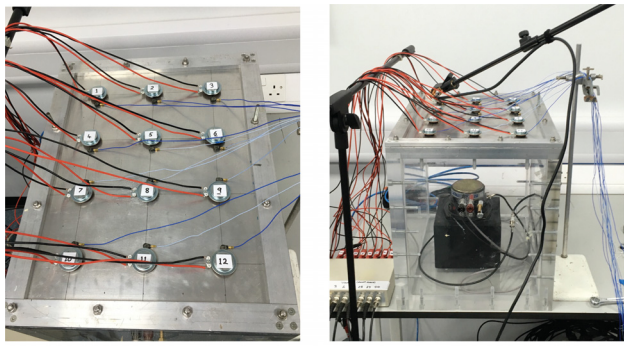

FIG. 4. (Color online) Photographs showing the plate mounted to a rigid enclosure which contains the primary disturbance, a volumetric loudspeaker (b). Fixed to the surface of the plate are 12 equally spaced actuators, each approximately collocated with an accelerometer (a).

B. Estimation of radiated sound power

To first identify the radiation resistance matrix, each of the actuators was driven independently with broadband white noise, and the structural and acoustic responses were measured. Using these responses to form the structural and acoustic transfer response matrices, the radiation resistance matrix was identified according to the formulation in Sec. II. The disturbance loudspeaker enclosed in the sealed cavity below the plate, shown in Fig. 4(b), was then used to excite the plate acoustically with broadband white noise. The radiated sound power was next calculated directly using the measured pressure and particle velocities as in Eq. (1), using both the radiation resistance matrix estimated with the method formulated in Sec. II and the positive semi-definite approximant of the radiation resistance matrix. Figure 5 shows the measured sound power and the two estimates.

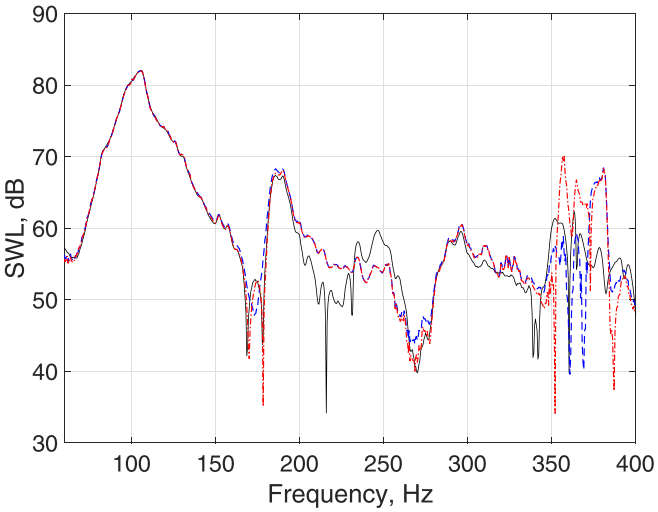

FIG. 5. (Color online) Sound power radiated from the plate shown in Fig. 2 when acoustically excited using white noise. The solid black line shows the directly measured sound power, and the dashed blue and dotted-dashed red lines show the sound power estimates calculated using the radiation resistance matrix and the positive semi-definite approximant of the matrix, respectively.

From these results it can be seen that, over the presented frequency range, the sound power estimated using the radiation resistance matrix and the positive semi-definite approximant of the matrix are approximately equivalent and both accurately estimate the directly measured sound power. The main differences between the estimates and the directly measured sound power occur at frequencies above 350 Hz, where the number of sensors and forces compared to the acoustic wavelength reaches the limit identified in Ref. 12.

1. Robustness study

It has been assumed in the sound power estimations presented in Fig. 5 and previously in Ref. 12 that there is no uncertainty in the response measurements used to calculate the radiation resistance matrix. In practice, it is likely that the nominal measured responses used to identify the radiation resistance matrix will be subject to some level of uncertainty since the physical responses will change over time depending on the operational conditions. This could affect the accuracy of the sound power estimate and, consequently, the performance of the ASAC strategy. To assess the robustness of the sound power estimate, a level of random error has been introduced into the transfer response matrices and its effect on the sound power estimate has then been evaluated. Each transfer response with uncertainties in both its magnitude and phase can be expressed as

$$h_{lm} = \Delta_n h_{0_{lm}} e^{j\phi_n}, \tag{26}$$

where $h_{0_{lm}}$ is the nominal transfer response between actuator, m, and accelerometer, l, and Δ_n and ϕ_n are bounded normally distributed random numbers used to introduce a level of uncertainty into the magnitude and phase of the response, respectively.

In the following, three different levels of random uncertainty are introduced into the structural and acoustic transfer responses, as per Eq. (26) For each level of uncertainty, this process was repeated 100 times to enable a statistical analysis of how random uncertainties influence the sound power estimation and, subsequently, the control performance. Table I shows the upper and lower bounds of the normally distributed noise introduced into the magnitude and phase of the transfer response for each level of uncertainty.

To provide an illustration of how the assumed uncertainties influence the nominal responses, Fig. 6 shows the magnitude and phase of the nominal transfer response between actuator eight and accelerometer five, which correspond to

TABLE I. The upper and lower bounds on the normally distributed noise introduced into the magnitude and phase of the transfer response for each level of uncertainty.

Uncertainty, n	Magnitude, Δ (dB)	Phase, ϕ (°)
1	±1	±5
2	±3	±15
3	±6	±30

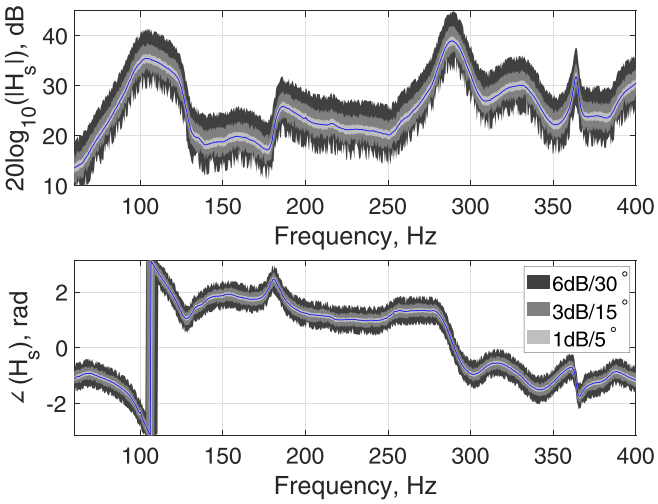

FIG. 6. (Color online) Magnitude and phase of the transfer response between actuator eight and accelerometer five. The nominal response is shown by the solid blue line, and the upper and lower limits of 100 responses with added uncertainty are shown by the shaded regions.

the two inner positions on the plate as shown in Fig. 4 The shaded regions around the nominal response show the upper and lower limits of the perturbed responses based on 100 iterations of the random uncertainties. Independent uncertainty was also added to the acoustic transfer responses using the same process and bounds as for the structural response uncertainties.

Figure 7 shows the sound power estimated using the radiation resistance matrix with no error, along with three shaded regions which show the range in the error in the sound power estimate up to the 75th percentile for the three levels of uncertainty described in Table I. For the lowest level of uncertainty, (±1 dB and 5°), it can be seen from these results that the sound power estimate is robust to the uncertainties in the transfer responses up to approximately

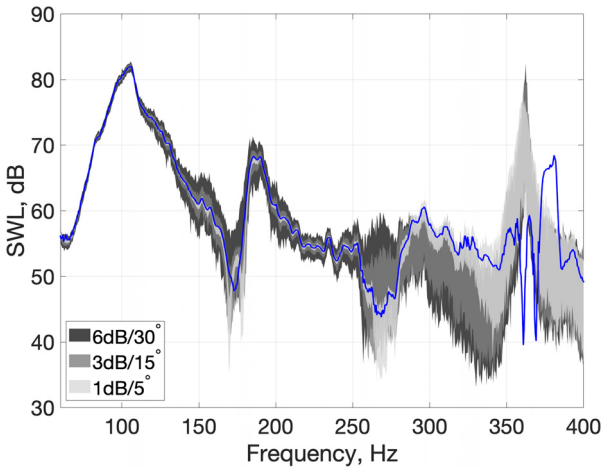

FIG. 7. (Color online) Sound power estimate calculated using the radiation resistance matrix. The blue line shows the estimate calculated using the transfer response matrices with no uncertainty. The shaded regions show up to the 75th percentile range of errors introduced into the estimate when 100 normally distributed uncertainties of 3 differing levels were introduced into the 3 transfer response matrices.

https://doi.org/10.1121/10.0000858

320 Hz. At higher frequencies, the range of error in the estimate increases as the upper frequency limit of the sound power estimate has been exceeded at around 350 Hz. As the level of uncertainty is increased to 3 dB and 15°, the range of errors in the sound power estimate at lower frequencies increases. However, the estimate remains accurate to within 2 dB up to approximately 250 Hz. Above 250 Hz, the range of the error in the sound power estimate increases and is in excess of 10 dB above 300 Hz. Increasing the level of uncertainty in the transfer responses further results in a wider range of error in the sound power estimate, and the frequency at which the estimation errors begin to exceed 10 dB is reduced to around 250 Hz. These results show that the sound power estimate is more robust to uncertainties of the assumed form in the transfer responses at lower frequencies. At higher frequencies, as the sound power estimate approaches the upper frequency limit defined by the source and sensor spacing, uncertainties in the transfer responses have a greater effect on the accuracy of the sound power estimate. Larger levels of uncertainty in the transfer responses result in larger errors in the sound power estimate and a decrease in the upper frequency at which the sound power estimate is reasonably accurate.

C. Optimal tonal control

The responses described in Sec. IV B and used to identify the radiation resistance matrix have been used to simulate optimal control of the plate for both AVC and the proposed ASAC strategy. The vector of optimal control signals for each strategy was calculated according to Eqs. (12) and (24) at each frequency over the range 60–400 Hz. The regularization term in each case was set according to Eq. (14), with α and γ set to ensure the quickest possible stable convergence for the real-time adaptive controllers defined by Eqs. (13) and (25).

Figure 8 shows the sum of the squared error signals measured on the surface of the plate and the radiated sound power estimate for each control strategy before and after control. These results show that, over the presented frequency range, AVC achieves a greater reduction in the structural response than ASAC, which at some higher frequencies actually increases the level of the structural response. In terms of the sound power estimate, at lower frequencies, where the coupling between the structural response and the radiated sound power is stronger, ASAC and AVC achieve a similar level of sound power control. However, above approximately 175 Hz, ASAC achieves a much higher level of attenuation in the radiated sound power than AVC. Above 255 Hz, AVC in fact struggles to achieve more than approximately 5 dB attenuation and increases the radiated sound power at some frequencies.

1. Robustness study

To assess the robustness of each control strategy to differences between the physical and estimated plant

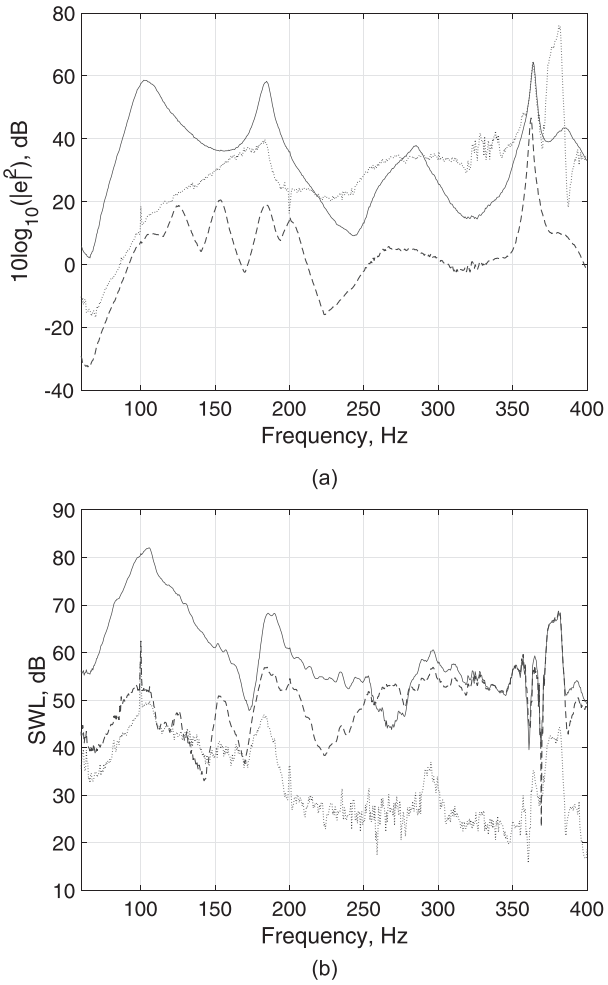

FIG. 8. The sum of the squared error signals (a) and estimated sound power (b) when the optimal control for both AVC (dashed line) and the proposed ASAC strategy (dotted line) was implemented, plotted along with the uncontrolled response (solid line).

responses, random error was introduced into each control system via inclusion of three different levels of normally distributed random errors in the magnitude and phase of the measured transfer responses, as in Sec. IV B 1. For AVC, the uncertainties were introduced into the structural plant estimate, $\widehat{\mathbf{G}}$, shown in the block diagram in Fig. 2. In the ASAC system, the uncertainties were introduced into both the structural plant estimate and the transfer responses that were used to identify the estimated radiation resistance matrix, $\widehat{\mathbf{R}}$, as in Sec. IV B 1.

Figure 9 shows the uncontrolled structural response plotted along with the controlled structural response for both AVC and ASAC, and Fig. 10 shows the uncontrolled sound power estimate plotted along with the controlled sound power estimate for both AVC and ASAC. The shaded regions in each plot show the range of attenuation achieved, up to the 75th percentile, when control was simulated for 100 iterations of the perturbed plant responses and radiation resistance matrix for the 3 levels of uncertainty.

From the results presented in Figs. 9 and 10, it can be seen that AVC is robust to 1 dB and 5° of uncertainty

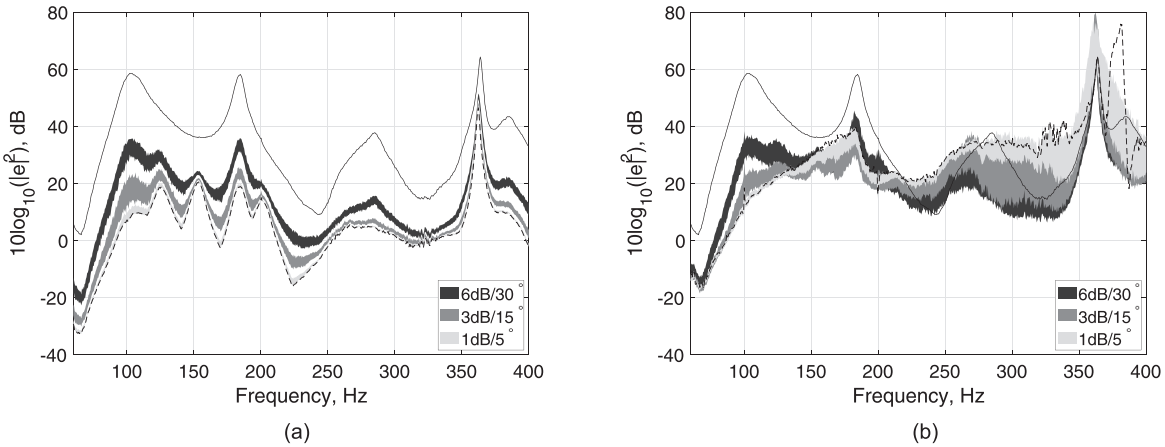

FIG. 9. The sum of the squared error signals before (solid black line) and after (dashed black line) optimal control for both AVC (a) and the proposed ASAC strategy (b). The shaded regions indicate the range of optimal control achievable when differing levels of uncertainty were introduced into the structural plant responses $\widehat{\mathbf{G}}$ and $\widehat{\mathbf{R}}$.

across the presented frequency range, losing no more than approximately 3 dB attenuation in either the structural response or the estimated sound power. For the proposed ASAC strategy, 1 dB and 5° of uncertainty also reduces the sound power attenuation performance at frequencies lower than 250 Hz by no more than approximately 3 dB, and the overall level of sound power attenuation remains greater than that of AVC. As the control frequency approaches the upper frequency limit of the radiation resistance matrix, there is an increased reduction in the sound power attenuation performance and the range of levels of attenuation also widens, resulting in an enhancement in the sound power level at frequencies above around 350 Hz. Although these results demonstrate that the performance of the ASAC system is more sensitive to uncertainties than AVC, it is important to note that the level of sound power attenuation achieved is greater than that of AVC up to 350 Hz. Above 350 Hz, the approximate limit of the radiation resistance matrix identification procedure, ASAC results in an increase in the estimated sound power.

As the level of uncertainty is increased to 3 dB and 15° and then 6 dB and 30°, the range of variation in the controlled structural response and sound power estimate for the AVC system increases slightly and the overall level of attenuation decreases, apart from above approximately 280 Hz, where there is little to no variation in the controlled sound power estimate. Increasing the uncertainty in the proposed ASAC system also widens the range of the controlled sound power estimate and reduces the overall level of attenuation. However, the increase in range and decrease in overall attenuation is greater than that of AVC. This is because uncertainties are introduced via both the structural plant response, $\widehat{\mathbf{G}}$, and the radiation resistance matrix, $\widehat{\mathbf{R}}$ It is clear from this investigation that uncertainties in the practical system should be considered when designing a practical ASAC system. In particular, it is clear that the performance rapidly decreases at frequencies greater than the upper limit of the radiation resistance matrix identification method and, therefore, the proposed ASAC strategy should not be applied at frequencies outside of its intended operating range.

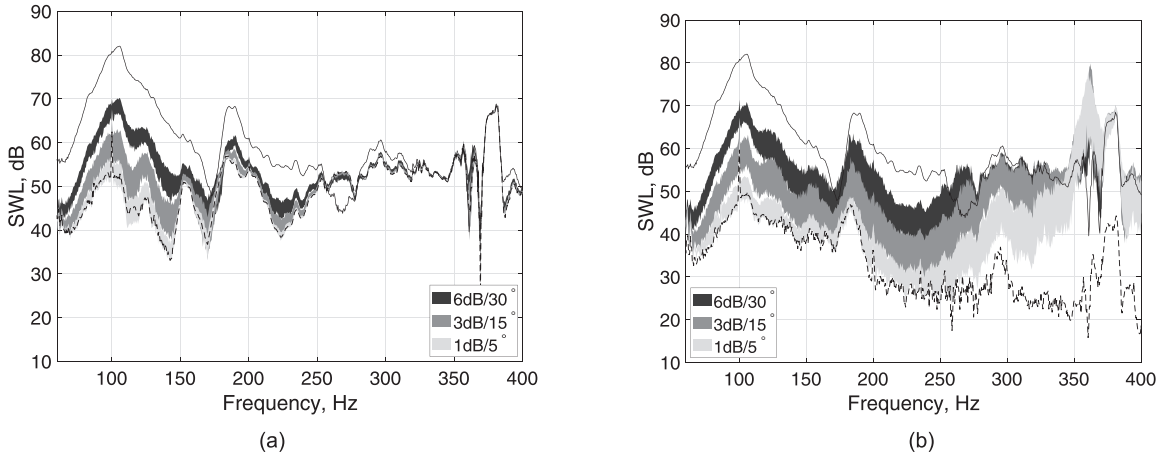

FIG. 10. The estimated sound power before (solid black line) and after (dashed black line) optimal control for both AVC (a) and the proposed ASAC strategy (b). The shaded regions indicate the range of optimal control achievable when differing levels of uncertainty were introduced into the structural plant responses $\widehat{\mathbf{G}}$ and $\widehat{\mathbf{R}}$.

https://doi.org/10.1121/10.0000858

V. EXPERIMENTAL VALIDATION

In this section, results are presented for the AVC and proposed ASAC strategies implemented in real-time to control, respectively, the vibration and radiation of the plate shown in Fig. 4 when it is excited tonally at discrete frequencies. Four frequencies were selected for this study, corresponding to resonances at 106 Hz, which is the breathing mode of the plate; 186 Hz, which is the (1,3) mode; and 297 Hz, which is the (3,1) mode; and one off-resonance frequency of 263 Hz. Using the same control hardware as described in Sec. IV A, the plate was excited acoustically at each frequency using a loudspeaker in the sealed cavity beneath the plate. Each control strategy was then implemented in real-time using the feedforward control architectures described in Sec. III. The convergence gain and leakage factors for each controller were set to ensure the quickest stable convergence.

Table II shows the attenuation achieved in each of the cost functions, J_s and J_W, as well as the directly evaluated sound power after convergence at each frequency for the two control strategies. These results validate the offline results presented in Sec. IV C with a clear performance advantage in terms of the sound power control achieved by the proposed ASAC strategy over AVC. Importantly, the results in Table II also show that the sound power estimate being minimised by the ASAC system, J_W, matches the directly measured sound power within 2 dB for the lowest three frequencies. At 297 Hz, however, the sound power is underestimated by 4 dB for the ASAC strategy, and this is thought to be related to the errors inherent in the estimation of the radiation resistance matrix that is used in the controller and the increased sensitivity to practical uncertainties at higher frequencies in the ASAC controller, as shown in Sec. IV C 1.

VI. CONCLUSIONS

This paper has proposed and investigated the performance of a tonal ASAC strategy that utilises an experimentally identified radiation resistance matrix to control the sound power radiated from a structure using only structurally located error sensors and control actuators. The proposed ASAC strategy was investigated through both simulations and experimental implementation for the flat plate. The performance and robustness of the proposed ASAC strategy was assessed via comparison to that of an AVC system that utilises the same control hardware. Both the simulated and experimental results have shown that at lower frequencies, the sound power attenuation performance of the two strategies is comparable; however, as the frequency of the radiated sound increases, the proposed ASAC strategy is able to provide significantly higher levels of sound power attenuation compared to AVC. Thus, this validates the proposed ASAC strategy as an effective method for controlling radiation from vibrating structures where it is not otherwise straightforward to relate the structural response to the radiated acoustic response.

Whilst the study presented has demonstrated the potential of the proposed ASAC strategy, there are also several areas of interest that would require further investigation for practical implementation of the strategy on a larger scale. It is evident that the number of forces, and therefore, actuators, required for this setup could quickly grow very large when scaling the setup for larger radiating structures. Although the number of forces used in this study is required for the identification of the radiation resistance matrix, $\widehat{\mathbf{R}}$, it is not necessarily needed for the actual control aspect. Therefore, in order to reduce the number of permanent actuators required by the system, further work will investigate the use of temporary structural excitation to perform the identification process. Similarly, the number of structural sensors has the potential to increase significantly in scaling up for larger structures and, therefore, future work could investigate the use of remote sensing techniques in the controller to reduce the number of permanent structural sensors required by the system. Following these advancements, the identification and control of more complex structures will be investigated in future work. Additionally, the work presented in this paper has only considered the tonal control problem, and for a variety of practical problems this should be extended to the control of broadband disturbances.

TABLE II. The attenuation of the structural cost function, J_s, sound power cost function, J_W, and the measured sound power, W, for each control strategy.

Frequency	Strategy	J_s (dB)	J_W (dB)	W (dB)
106 Hz	AVC	−24	−29	−30
	ASAC	−22	−32	−30
186 Hz	AVC	−19	−13	−13
	ASAC	−11	−15	−17
263 Hz	AVC	−10	+3	+4
	ASAC	+3	−13	−13
297 Hz	AVC	−13	−4	−4
	ASAC	+3	−22	−26

ACKNOWLEDGMENTS

This research was partially supported by an Engineering and Physical Sciences Research Council (EPSRC) industrial Cooperative Award in Science and Technology (iCASE) studentship (Voucher No. 15220040) and an EPSRC Prosperity Partnership (EP/S03661X/1). All data supporting this study are openly available from the University of Southampton repository at https://doi.org/10.5258/SOTON/D1259.

[1]F. Fahy and P. Gardonio, *Sound and Structural Vibration* (Academic, Oxford, 2007).
[2]W. T. Baumann, F.-S. Ho, and H. H. Robertshaw, "Active structural acoustic control of broadband disturbances," J. Acoust. Soc. Am. **92**(4), 1998–2005 (1992).
[3]J. Cheer and S. Daley, "Active structural acoustic control using the remote sensor method," J. Phys.: Conf. Ser. **744**(1), 012184 (2016).
[4]S. Elliott and M. E. Johnson, "Radiation modes and the active control of sound power," J. Acoust. Soc. Am. **94**(4), 2194–2204 (1993).

[5]O. Janda, G. L. Stein, U. Konigorski, and O. Heuss, "Identification of power transfer matrices for active structural acoustic control," in *20th International Congress on Sound and Vibration, ICSV20* (2013).
[6]A. P. Berkhoff, "Broadband radiation modes: Estimation and active control," J. Acoust. Soc. Am. **111**(3), 1295–1305 (2002).
[7]D. R. Hendricks, W. R. Johnson, S. D. Sommerfeldt, and J. D. Blotter, "Experimental active structural acoustic control of simply supported plates using a weighted sum of spatial gradients," J. Acoust. Soc. Am. **136**(5), 2598–2608 (2014).
[8]P. Aslani, S. D. Sommerfeldt, and J. D. Blotter, "Active control of simply supported cylindrical shells using the weighted sum of spatial gradients control metric," J. Acoust. Soc. Am. **143**(1), 271–280 (2018).
[9]J. B. Fahnline and G. H. Koopmann, "A lumped parameter model for the acoustic power output from a vibrating structure," J. Acoust. Soc. Am. **100**(6), 3539–3547 (1996).
[10]J. B. Fahnline and G. H. Koopmann, "Numerical implementation of the lumped parameter model for the acoustic power output of a vibrating structure," J. Acoust. Soc. Am. **102**(1), 179–192 (1997).
[11]G. H. Koopmann and J. B. Fahnline, *Designing Quiet Structures: A Sound Power Minimization Approach* (Academic, London, 1997).
[12]J. Milton, J. Cheer, and S. Daley, "Experimental identification of the radiation resistance matrix," J. Acoust. Soc. Am. **145**(5), 2885–2894 (2019).
[13]L. E. Kinsler, A. R. Frey, J. V. Sanders, and A. B. Coppens, *Fundamental of Acoustics* (Wiley, New York, 1999).
[14]J. Milton, J. Cheer, and S. Daley, "An inverse method for the identification of the radiation resistance matrix from measurable acoustic and structural responses," in *25th International Congress on Sound and Vibration* (2018).
[15]J. Milton, J. Cheer, and S. Daley, "Active structural acoustic control of a flat plate using an experimentally identified radiation resistance matrix," in *26th International Congress on Sound and Vibration* (2019).
[16]R. Pintelon and J. Schoukens, *System Identification: A Frequency Domain Approach* (Wiley, New Jersey, 2012).
[17]S. J. Elliott, *Signal Processing for Active Control* (Academic, London, 2000).
[18]N. J. Higham, "Computing a nearest symmetric positive semidefinite matrix," Linear Algebra Appl. **103**, 103–118 (1988).
[19]C. F. V. Loan and G. H. Golub, *Matrix Computations* (Johns Hopkins University Press, London, 1983).
[20]BS EN ISO 9614-1:2009: *Acoustics–Determination of Sound Power Levels of Noise Sources using Sound Intensity—Part 1: Measurement at Discrete Points* (British Standards Institution, London, 2009).